THESIS FOR THE DEGREE OF LICENTIATE OF ENGINEERING

Novel approaches for monitoring effects of steel corrosion in reinforced concrete

ANDREAS ALHEDE

Department of Architecture and Civil Engineering

Division of Structural Engineering

CHALMERS UNIVERSITY OF TECHNOLOGY

Gothenburg, Sweden 2023

Novel approaches for monitoring effects of steel corrosion in reinforced concrete
ANDREAS ALHEDE

Division of Structural Engineering
Department of Architecture and Civil Engineering
Chalmers University of Technology
SE-412 96 Gothenburg
Sweden
Telephone: +46 (0)31-772 1000

Cover
Reinforced concrete revealed by Neutron Computed Tomography and corrosion-induced deformations within concrete (coloured vector field)

Novel approaches for monitoring effects of steel corrosion in reinforced concrete
Thesis for the degree of Licentiate of Engineering

ANDREAS ALHEDE

Department of Architecture and Civil Engineering
Division of Structural Engineering
Chalmers University of Technology

ABSTRACT

Corrosion of steel reinforcement is a common deterioration mechanism in reinforced concrete structures. This deterioration impacts the safety of the structure and may require extensive repair and maintenance work. There is currently no method available for accurately measuring internal corrosion damage non-destructively. Therefore, establishing correlations between outer signs of corrosion, such as crack pattern and width, and the corresponding internal corrosion morphology and level is of significant interest. However, prior research has shown that relying solely on crack width as a performance indicator for corrosion damage is inadequate. Hence, further research is needed to study the corrosion and cracking processes in reinforced concrete to be able to identify and quantify underlying physical processes and factors. To contribute to knowledge in the field, this thesis focuses on novel approaches for non-destructive monitoring of the effects of steel corrosion in small-scale reinforced concrete samples.

In this work, time-resolved neutron and X-ray Computed Tomography were applied to link the evolution of material phases to kinematics. Further, two independent studies, one using neutron and the other using X-ray Computed Tomography, were used to quantify corrosion-induced deformations within concrete. These deformations were successfully quantified, and the identified locations of concrete cracking correlated well with the observed strain localisation. Interestingly, the kinematics quantified allowed for the detection of strain localisation in areas where concrete cracks were too small to be visually identified from the image data, indicating the potential for early-stage concrete crack detection. Additionally, an expression for the average volumetric strain in the compressed corrosion layer was derived based on the evolution of material phases within the sample.

Further, an experimental setup was designed to monitor corrosion-induced deformations adjacent to the steel-concrete interface using an open-ended steel tube instrumented with an optical fibre for distributed strain sensing. X-ray Computed

Tomography allowed for quantitative and qualitative assessment of corrosion level and concrete cracking. The corrosion-induced deformations in the steel tube were found to be non-uniform, indicating a non-uniform distribution of radial stress around the steel. This non-uniformity correlated well with the location of the corrosion-induced cracks, with extension hoop strains observed in the steel tube at the location of these cracks, and contraction hoop strains observed in between them. Corrosion was more severe in bands along the steel, coinciding with the position of the longitudinal cracks.

The research conducted in this work demonstrated the potential of non-destructive monitoring of steel corrosion in reinforced concrete. For future research aiming at increasing the fundamental understanding of corrosion-induced concrete cracking, it is essential to integrate advanced experimental techniques with numerical modelling.

To my parents

Preface

The work presented in this thesis was conducted at the Division of Structural Engineering at Chalmers University of Technology between October 2020 and May 2023. The project was financially supported by the Swedish Research Council for Sustainable Development (Formas) and the Swedish Transport Administration (Trafikverket).

I would like to express my sincere appreciation to my supervisor, Professor Karin Lundgren, for her continuous support and dedication to my research education. Her guidance and engagement have been invaluable throughout this journey. I would also like to extend my gratitude to my co-supervisor, Professor Jelke Dijkstra, for his expertise and guidance in the experimental work carried out in this thesis. I am grateful to both of you for all discussions that enabled this work. The discussions and teamwork with both of you have been instrumental in the success of this research. I eagerly anticipate the opportunity to continue our collaboration towards my PhD.

Furthermore, I would like to express my appreciation to all my colleagues for creating a friendly and pleasant atmosphere. Our engaging conversations and idea-sharing during coffee breaks have been invaluable. I am especially thankful to Senior Research Engineer Sebastian Almfeldt and Research Engineer Anders Karlsson for their assistance in the lab. Their support is greatly acknowledged.

I would also like to express my gratitude to every member of the reference group. A special thanks to Katja Frid, Head of Department at Malmö University, for her keen interest in my research, and for generously sharing her expertise in material science.

Lastly, I owe a debt of gratitude to my family, whose unwavering love and support have kept me motivated through the mental ups and downs of pursuing a PhD. Thank you for your belief in me and for allowing me to live my life on my own terms.

Tack

Andreas Alhede

Gothenburg, 2023

LIST OF PUBLICATIONS

This thesis presents a summary and an extension to the following appended papers:

[I] A. Alhede, J. Dijkstra, S. Robuschi, A. Tengattini, and K. Lundgren. *Reinforced concrete: evolution of steel corrosion and internal cracking revealed by 4D multimodal tomography.* Submitted for publication. (2023).

[II] A. Alhede, J. Dijkstra, and K. Lundgren. *Inside out: monitoring corrosion-induced concrete cracking adjacent to the steel-concrete interface.* Submitted for publication. (2023).

These publications are always referred to as paper I and II, according to the labeling in the list above.

AUTHOR'S CONTRIBUTION TO JOINTLY WRITTEN PAPERS

The appended papers were prepared in collaboration with co-authors. In the following, the contribution of the author of this thesis to the appended papers is outlined.

In **Paper I**, the author contributed to the formulation of the research aim, carried out analyses, constructed figures and took responsibility for the planning and writing the first draft of the paper.

In **Paper II**, the author contributed to the formulation of the research aim, participated in the planning, and was responsible for execution of the experimental programme. The author was also responsible for pre- and post-processing of the data and participated in the discussion of data visualisation. The author also wrote the first draft of the paper.

CONTENTS

1 Introduction

1.1 Background

Concrete is among the oldest and most consumed construction materials in the world [1]. The archaeological site of Tiryns, Greece, has revealed findings of concrete slabs dating back to 1400 - 1200 BC [2]. The use of reinforced concrete dates back to the 19th century, when Joseph Monier pioneered the approach of casting iron into concrete to increase the tensile strength of the structural element [3]. Currently, reinforced concrete is extensively used worldwide in a variety of civil infrastructure applications, such as in buildings, bridges, offshore constructions, tunnels and foundations, among others.

The durability of reinforced concrete structures is governed by the exposure conditions, which differ depending on the application area. The most common deterioration mechanism for reinforced concrete structures is the corrosion of steel reinforcement [4]. Structures exposed to high concentrations of chlorides, e.g. in seawater or de-icing salts, are particularly susceptible to steel corrosion [5]. Oxidation of steel into corrosion products leads to a reduction of steel cross-sectional area, loss of ductility, concrete cracking and a loss of bond between the steel and the concrete [6]. Once the corrosion process has been initiated, it progresses over time. Consequently, extensive repair and maintenance work may be required to ensure the structural safety of the affected structure. In 2013, it was estimated that the annual direct corrosion cost of civil infrastructures in the United States was \$20.5 billion [7]. In China, the estimated cost of corrosion in 2014 was 62 billion RMB (\$9.1 billion) [8]. Several studies have shown that ongoing climate change increases the risk of corrosion in reinforced concrete structures [9–11]. A recent study estimated that the probability of corrosion initiation among reinforced concrete structures in Sweden could increase up to 33% by the end of the twenty-first century due to climate change [12]. Thus, the climate change is expected to increase the occurrence of corrosion damage in reinforced concrete structures in the future.

A proper assessment of the corrosion damage is essential to enable safe use of corroded RC structures. This allows for targeted measures to be taken, potentially leading to substantial reduction in costs. Extensive research has been carried out on the assessment of corrosion damage in engineering structures. Electric potential measurements can be applied to detect an active oxidation process and the corresponding corrosion zone [13], and there are various methods available

to monitor the instantaneous corrosion rate in steel reinforcement [14]. However, the intrinsic factors affecting the corrosion rate change over time due to variations in exposure conditions, among others [15], and current research emphasises the importance of developing reliable non-destructive, monitoring techniques [16].

In addition to research on techniques for monitoring corrosion-induced cracking of reinforced concrete, studies have been performed to identify performance indicators of corrosion damage that can be used for on-site structural health assessment. For example, several studies have investigated the probable relationship between surface crack width and corrosion level, see [17–24]. The potential benefit of such a relationship is that the internal corrosion damage could be assessed through visual inspections without the need for destructive actions. However, this experimental relationship between surface crack width and corrosion level has shown large uncertainties [20, 21]. This indicates that only linking crack width to corrosion level for assessment of the corrosion damage is insufficient, and that other factors with important influence on the corrosion-induced cracking process, for example corrosion morphology, type of corrosion products and transport of corrosion products through pore networks and cracks, need to be considered.

New non-destructive methods that enable the characterisation of evolving processes on the steel-concrete interface (SCI) with sufficiently high spatial resolution are essential for advancing the field. Through the integration of advanced experimental methods with sophisticated numerical modelling, these approaches enhance the fundamental understanding of steel corrosion and its structural effects on reinforced concrete.

One existing method that is applicable for studying the corrosion process in reinforced concrete on a micro-structural level includes 3D imaging techniques, such as Neutron and X-ray Computed Tomography (NCT, XCT), see for example [25, 26]. The great opportunity of these techniques is that they are non-destructive, non-invasive and provide image data that allows for quantitative and qualitative measurements of the corrosion process in small-scale samples. In addition to 3D imaging techniques, steel corrosion in concrete has also been studied using distributed optical fibres systems [27].

1.2 Aim and objectives

The overall aim of the PhD project is to monitor and quantify the evolving physical processes involved in corrosion-induced cracking in reinforced concrete.

The following objectives were identified for this part of the project:

1. To quantify corrosion-induced deformations within concrete (**Paper I** and feasibility study)

2. To link the evolution of material phases to kinematics (**Paper I**)

3. To design an experimental setup, enabling monitoring of mechanical effects resulting from steel corrosion in reinforced concrete adjacent to the SCI, and subsequently execute an experimental programme to study the relation between corrosion-induced deformations in the steel, concrete cracking and corrosion level (**Paper II**)

1.3 Methodology

The research was structured to meet the outlined objectives. An overview is shown in Fig. 1.1.
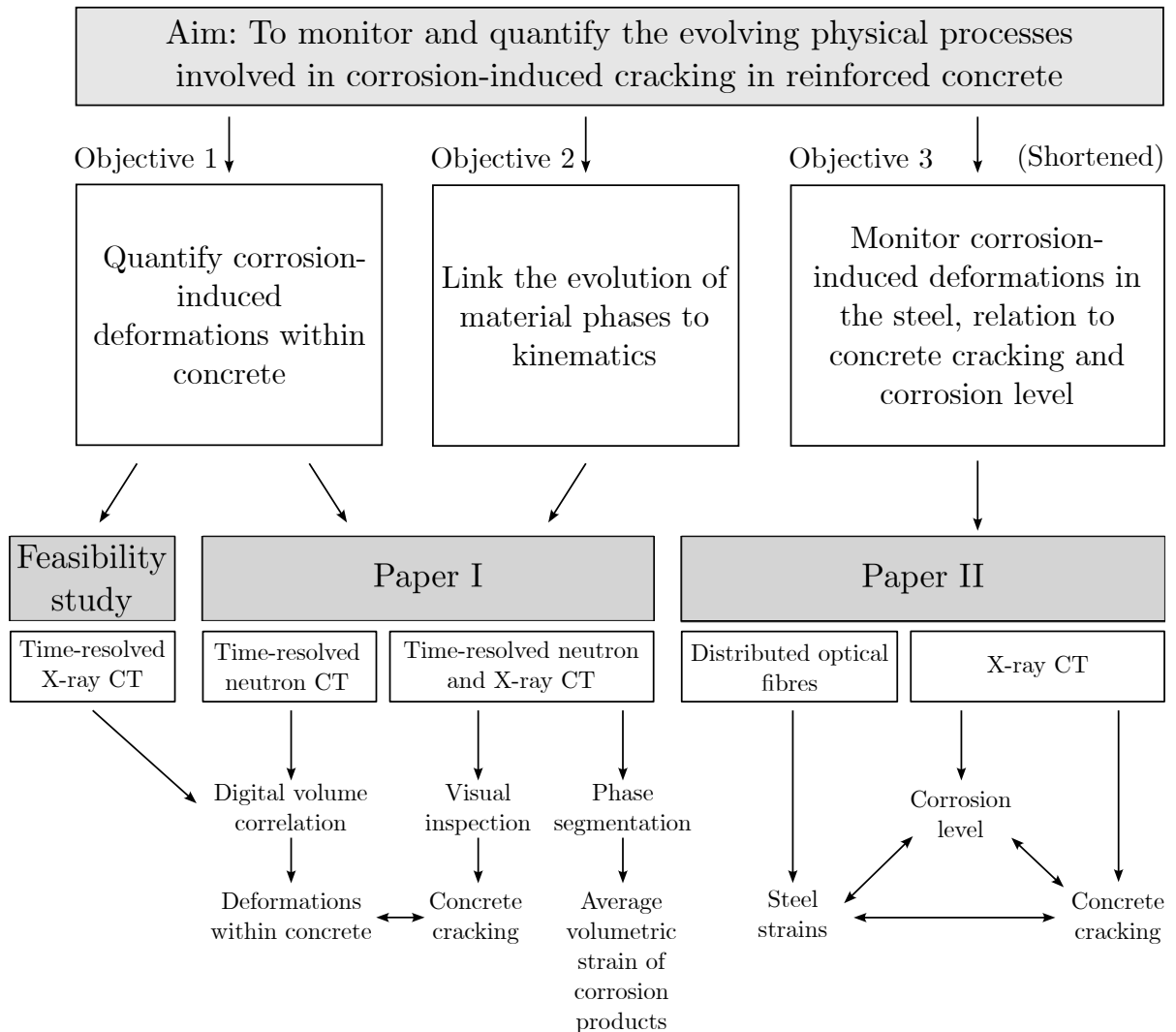

Figure 1.1: *Overview of connections between the overall aim of the PhD project, objectives for this part of the project and the work conducted.*

In **Paper I**, one small-scale reinforced concrete sample was subjected to accelerated corrosion and changes in the sample was monitored using data from

multimodal NCT and XCT scans. Two scans were carried out, with additional corrosion propagation in between. Several analyses were performed for which the interplay between concrete cracking and kinematics in the concrete cover were studied. Moreover, phase segmentation of the sample allowed for derivation of an expression for the average volumetric strain in the compressed corrosion layer (Chapter 3).

In **Paper II**, an experimental setup was designed aiming at studying the relation between corrosion-induced deformations in the steel, concrete cracking and corrosion level. Subsequently, an experimental programme was designed and executed. The programme included four different test types with small-scale samples, reinforced with a hollow steel tube, of which three were subjected to accelerated corrosion. Corrosion-induced deformations of the inner surface of the steel tube were monitored using a distributed optical fibres system. After the corrosion phase, XCT was used to acquire data from the inside of the specimens, thus allowing examination of concrete cracking and quantification of the corrosion level (Chapter 5).

In addition to the work conducted in **Papers I & II**, this thesis also includes a feasibility study on the applicability of time-resolved XCT in conjunction with digital volume correlation to non-invasively measure corrosion-induced deformations within the surrounding concrete (Chapter 4).

1.4 Limitations

Most limitations in this work are related to active choices made. The research is limited to small-scale laboratory made reinforced concrete specimens. Corrosion was imposed through an electrical current (accelerated corrosion). Further, the work is limited to the corrosion propagation phase, i.e. the steel bars were depassivated prior to the experiments.

2 Corrosion-induced cracking of reinforced concrete

2.1 Corrosion of steel in reinforced concrete

Corrosion of steel reinforcement in concrete is an electrochemical process. For this process to occur naturally, two half-cell reactions, i.e. one anodic and one cathodic reaction, must be active [28]. In reinforced concrete, these reactions occur at the interface between the steel and the concrete, as seen in Fig. 2.1. The anodic reaction involves the oxidation of iron in the steel into iron ions and free electrons. These electrons are transported in the steel to be consumed in the cathodic reaction, together with oxygen [29]. This oxidation of steel in concrete is governed by the electrochemical potential at the surface of the steel and the pH of the pore solution of concrete [28]. The Pourbaix [30] diagram, shown in Fig. 2.2, schematically illustrates the possible phases for which the electrochemical system is thermodynamically stable. The first phase corresponds to the immunity region where corrosion is inhibited. The second phase encompasses two regions where corrosion can occur. The third phase represents the area where passivation of the steel is possible. In this region, a protective passive film consisting mainly of iron oxides forms on the surface of the steel. This film helps to prevent further corrosion, but can break due to chemical or mechanical factors. Prior to deterioration of reinforced concrete, the steel is typically in this region.
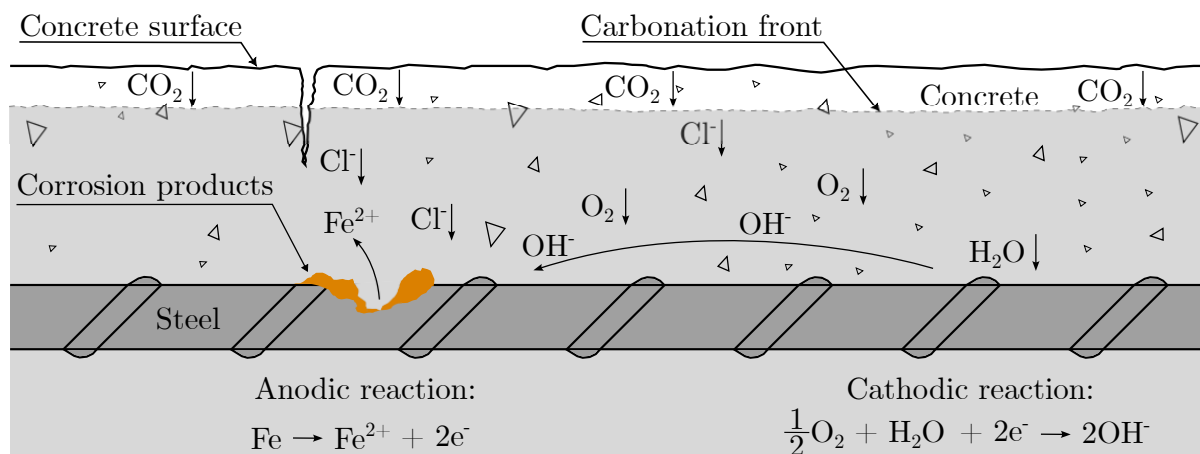

Figure 2.1: *Illustation of corrosion of steel reinforcement in concrete.*
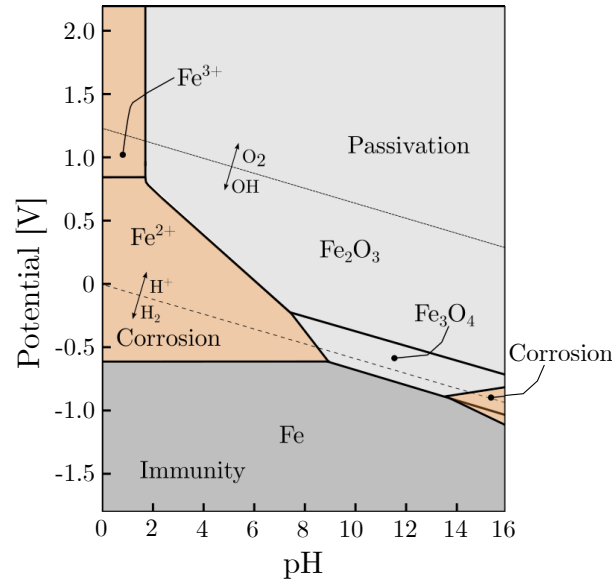
Figure 2.2: *A simplified version of the Pourbaix electrochemical potential - pH equilibrium diagram [30]. The diagram applies for iron and water, at a temperature of 25 °C.*

In reinforced concrete, two main mechanisms, chloride-induced and carbonation-induced corrosion, can disrupt the passive film on the steel [31]. The oxidation process can thereafter be triggered in presence of oxygen and hydrogen [32].

Transport of chloride ions in concrete is governed by diffusion [33], and at a certain chloride concentration at the level of the steel [34], corrosion is initiated by a local disruption of the passive layer. This chloride-induced corrosion results in pitting corrosion which significantly reduces the cross-sectional area of the steel locally [23], resulting in detrimental effects on the structural capacity of the element [35].

Carbonation-induced corrosion involves the diffusion of carbon dioxide into the pore network of the concrete where it reacts with calcium hydroxide to form calcite. Consequently, the pH of the pore water is reduced due to the depletion of hydroxyl ions [36]. Carbonation begins at the surface of the concrete and gradually penetrates into the depth of the concrete in presence of carbon dioxide [37]. When the carbonation front reaches the level of the steel, there is a shift from the passive region towards the corrosion region (see Fig. 2.2). Unlike chloride-induced corrosion, carbonation-induced corrosion is not as localised, as the carbonation front is more uniform, resulting in a larger area of the steel being depassivated.

In experimental research, corrosion is often induced using the galvanostatic method, which is an impressed current technique for accelerating corrosion where the corrosion rate depends on the current applied [38]. The current is applied to the anode (i.e. the reinforcing steel), while an external copper or stainless steel mesh serves as cathode. Faraday's law can be used to estimate the mass loss of

the steel in concrete when immersed in a saline solution during this accelerated corrosion process [39]. However, it should be noted that immersing the specimen in a saline solution during accelerated corrosion may result in different types of corrosion products compared to natural corrosion [40]. The effects of different corrosion products on the corrosion-induced cracking process are further discussed in Sec. 2.4.

The service life of a reinforced concrete structure with regards to corrosion can be divided into two different phases: initiation and propagation [31]. The initiation period corresponds to the period it takes for chlorides, carbon dioxide and other aggressive substances to depassivate the passive layer surrounding the surface of the reinforcing steel. The propagation period starts when the oxidation process becomes active [34].

2.2 Steel corrosion and its effects on reinforced concrete structures

There are several detrimental effects of steel reinforcement corrosion in concrete. The first effect, which was briefly discussed in Sec. 2.1, pertains to the loss of steel cross-sectional area which is a critical property for the ultimate capacity of the structure. In the case of chloride-induced corrosion, this reduction in steel area can be substantial in local areas of the bar, and depending on the location of induced pitting, the global response and fatigue performance [41] can be significantly reduced. Additionally, pitting corrosion reduces the tensile ductility of the steel [42, 43] which can affect the earthquake-resistance and the ability of the structure to undergo plastic redistribution [44]. For carbonation-induced corrosion, which results in a more general corrosion, the effects on load-carrying capacity and ductility are less severe.

The structural effects of reinforcement corrosion are not only limited to those of steel. Corrosion products occupy a larger volume than the original steel [31], as shown in Fig. 2.3. Since the steel is embedded in concrete, this free volume expansion cannot take place. Instead, stress-dependent volume expansion occurs, inducing splitting stresses and subsequent cracking of the concrete. If cracking occurs on the compressive side of the concrete cross-section, the size of the compressive zone, and consequently the ultimate capacity of the cross-section, is reduced [45]. Furthermore, corrosion of steel and cracking of concrete can lead to a reduction in bond strength [46], which can consequently affect the anchorage capacity.

2.3 The influence of concrete cracking on the corrosion process

The low tensile strength of concrete in engineering applications makes cracking inevitable. Cracks induced by external loads result in flexural and shear cracks that propagate in the transverse direction of the structural element. As these cracks can provide a pathway for the ingress of chlorides in existing structures, extensive research has been conducted to study the effect of cracking on the corrosion process and corrosion characteristics. In the following, a short overview of these studies is given.

While it is generally accepted that cracks can affect the initiation and propagation of steel corrosion, there is still limited knowledge on how certain factors, for example the size of the concrete cover, crack orientation and crack width, specifically influence the corrosion process [47]. Although it is likely for pitting corrosion to take place in the vicinity of pre-existing cracks [48, 49], no direct correlation between crack width and corrosion rate has been found. Conflicting findings regarding the effect of crack width on the corrosion process have been reported. For example, in [50], the corrosion rate was found to increase with an increase in chloride concentration at the level of the steel and an increase in crack width, while in [51, 52], the authors concluded that, for crack widths less than 0.5 mm, cracking had for the investigated time frame of 12 years no effect on the development of steel corrosion. In addition to studies on the influence of crack width on the corrosion process, conflicting results with regard to the influence of crack frequency on the corrosion rate have also been reported [47].

Cracks can also be induced by internal factors, for example steel corrosion. Previous research [53] claimed that pitting corrosion was responsible for driving these cracks, and further stated that the corrosion morphology becomes more uniform with an increase in crack width. Corrosion-induced cracks typically propagate along the reinforcing bar, as radial stresses are induced at the SCI, along the length of the steel. These cracks expose a large portion of the steel to aggressive substances [47] and are considered more severe for the corrosion of steel reinforcement compared to transversal cracks [22]. Some studies have found that the corrosion rate can increase if longitudinal cracks are present [54, 55], but no general relationship between longitudinal cracking and steel corrosion has been established.

2.4 Parameters influencing numerical prediction of corrosion-induced cracking in reinforced concrete

Modelling the process of corrosion-induced concrete cracking can facilitate the assessment of remaining structural capacity of existing structures. Various models have been proposed, see for example [56–59], where corrosion of steel reinforcement has been taken into account on different levels of detail. As a consequence of phenomenological modelling, calibration of corrosion characteristics is important. However, as oxides and their properties evolve with time and exposure conditions [60], this characterisation is challenging. Therefore, there is a need to develop non-destructive and non-invasive methods for monitoring the effects of corrosion of steel in reinforced concrete. In the following, some factors in corrosion modelling that have been considered in earlier work [57–59, 61], are introduced.

Volumetric expansion coefficient of corrosion products

As described in Sec. 2.2, the specific volume of corrosion products is larger than that of steel. This specific volume of corrosion products can be up to 2-6 times larger than the virgin steel [31], as shown in Fig. 2.3. Consequently, the time to concrete cracking is significantly affected by the type of corrosion formed at the SCI, and proper quantification of this factor is necessary to achieve realistic outputs from modelling. As introduced earlier, oxides and their properties evolve with time and exposure conditions [60]. Thus, there is a need for methods to characterise corrosion products of steel in reinforced concrete without destructive and invasive measures.
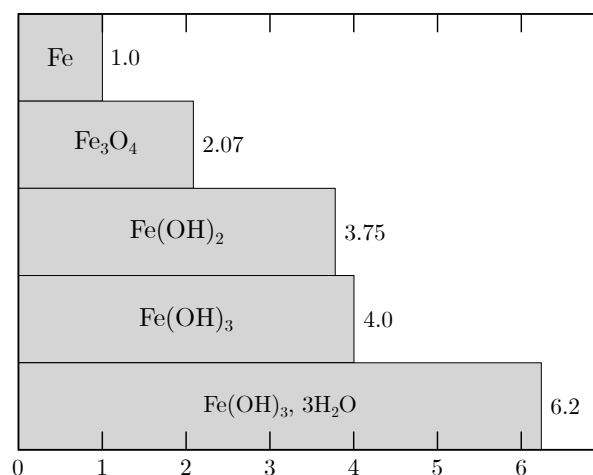

Figure 2.3: *Volumetric ratio between various types of corrosion products and iron. Modified from [31].*

Mechanical behaviour of corrosion products

In the constitutive modelling of the corrosion-induced cracking process, the mechanical properties of corrosion products are of significance. Previous research has applied different types of behaviour, such as linear elastic [59, 62, 63] and non-linear [58]. Experimental characterisation of the mechanics of corrosion products indicates a non-linear mechanical behaviour [64, 65]. However, since the corrosion particles were dried and exposed to ambient air prior to testing, the resulting oxides may have changed before testing, and therefore, the reported stress and strain relation may not accurately reflect the mechanics of corrosion products formed in reinforced concrete.

Corrosion accommodating region

In attempts to calibrate corrosion models to better fit experimental results of the corrosion-induced cracking, the concept of diffusion of corrosion products into voids was hypothesised [66]. This concept was later discussed in [57] to involve a porous zone, also known as the corrosion accommodating region (CAR) [67], where it was argued that the porosity of the cementitious matrix is higher in the transition zone from steel to concrete. Hence, accommodation of corrosion products in this transition zone delays the onset of expansive stresses in the concrete, thus delays the occurrence of cracking. The concept of the CAR has been reviewed in [68], where it was concluded that further research is needed to determine whether this phenomenon physically exists or if it is a pure fitting parameter used in numerical modelling.

Pitting and general corrosion

As already discussed in Sec. 2.1, there are two main mechanisms initiating corrosion of steel in concrete, chloride-induced and carbonation-induced corrosion. These two mechanisms lead to different corrosion morphologies, pitting and general corrosion, respectively. In order to assess the degree of corrosion damage among existing engineering structures using corrosion models, the anodic and cathodic regions need to be predefined. In the case of chloride-induced corrosion, further research is required to investigate the regions of the SCI where pitting corrosion occurs.

Other factors influencing the numerical prediction of corrosion-induced cracking of reinforced concrete

In this section, other factors influencing the numerical prediction of corrosion-induced cracking of reinforced concrete are briefly discussed. For example, the material properties of concrete, such as the Young's modulus, tensile strength and fracture energy, affect the magnitude of corrosion-induced stresses that the

concrete can sustain before cracking. Geometrical factors, such as the thickness of the concrete cover, steel bar diameter [69], as well as the specimen size [70] have also shown to influence the corrosion-induced cracking process. Additionally, factors such as corrosion rate [19], transport of corrosion products [59], and local characteristics at the SCI [71] can be important to consider.

2.5 Image-based methods for non-destructive studies of the corrosion-induced cracking process

A main focus in this thesis is the implementation of non-destructive imaging-based monitoring methods to study corrosion-induced concrete cracking. These methods include X-ray and Neutron Computed Tomography (i.e. XCT and NCT), that have the advantage to obtain 3D images without disturbing the sample, hence enabling monitoring changing processes with time in the same sample. The sensitivity of X-ray attenuation to the atomic number [72], therefore density variations within the sample enables differentiation between the concrete matrix, voids and steel. neutrons interact with the atomic nuclei [73] and are particularly sensitive to light elements, such as hydrogen, which facilitates identification of cement paste and corrosion products.

Beck et al. [74] pioneered the approach of applying XCT to study steel corrosion in mortar. Since then, this technique has been widely used for both qualitative and quantitative studies of corrosion and cracking in reinforced concrete. For example, in [67], time-resolved changes at the SCI have been studied using XCT. Qualitative measures on the concentration of corrosion products and the influence of cracking have been performed and the possibility of monitoring CAR was discussed. Later, in [75], this region has been studied for several samples of different configurations using XCT. It was found that corrosion products penetrated into the cementitious matrix and at the time of cracking, the depth of this region was approximately 0.22 mm. Interestingly, neither the electrical current nor the water to cement ratio showed any effect on the thickness of CAR.

Corrosion-induced cracking has been studied in [76] where multiple XCT scans were obtained at different stages in the corrosion process. Unlike the study in [75], no effect of accumulation of corrosion products into CAR was observed. However, they observed that discontinuities within the corrosion layer were formed after cracking, and a significant effect of transport of corrosion through cracks. Although no quantitative measures on the radial pressure due to corrosion were conducted, it could be argued that the phenomenon of corrosion products leaching out through cracks reduces this pressure, i.e. not all corrosion contribute to the build-up of stress at the SCI.

Research has also been conducted for quantitative assessment of the volumet-

ric expansion coefficient of corrosion products. In [25], it was discussed that the oxidation process might be non-stationary, as the type of corrosion formed in the corrosion test evolved with time. Early in the corrosion propagation phase, the volumetric expansion coefficient of the corrosion products reached its highest value (3.97). This coefficient decreased later to 2.71, but increased thereafter to 3.59. Although it is unclear from the study if corrosion was induced by impressed current, two independent research studies [26, 77] on accelerated corrosion showed an almost one-to-one agreement on measures of the volumetric expansion coefficient, 3.9 [77] and 3.91 [26]. To the best of the author's knowledge, only one study has been conducted to quantify the volumetric expansion coefficient of natural corrosion formed in an engineering structure. In this study [26], values of 4.13 and 4.24 have been reported.

3 A study combining Neutron and X-ray Computed Tomography

In **Paper I**, an experimental programme was conducted to study the evolution of material phases in a reinforced concrete specimen subjected to steel corrosion. The aim was to evaluate the potential of time-resolved Neutron and X-ray Computed Tomography (NCT and XCT) in calibration of micro-structural parameters in corrosion models by linking corrosion characteristics and kinematics in the process of corrosion propagation. One specimen was cast, cured and subsequently subjected to accelerated corrosion. Thereafter, the specimen was scanned twice, with multimodal NCT and XCT, and additional corrosion propagation in between, see Fig. 3.1.
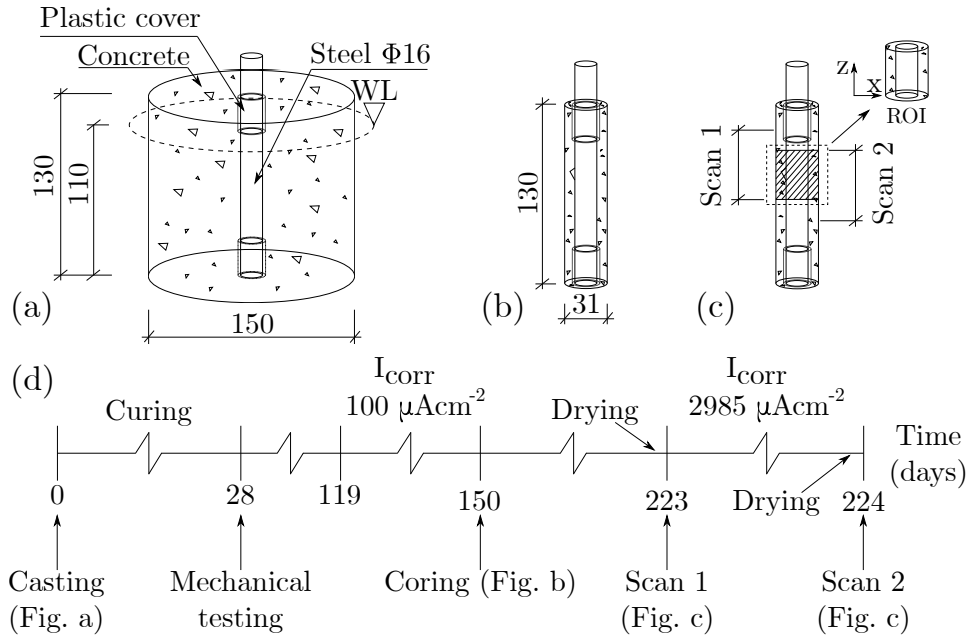
Figure 3.1: *Timeline and technical details of specimen. Measures in millimeter. a) Initial geometry at casting, curing and the first accelerated corrosion period. b) Geometry of specimen for the second period of accelerated corrosion. c) Regions scanned with NCT and XCT, including the Region of Interest (ROI). d) Timeline. Adopted from* **Paper I**.

13

3.1 Volumetric strain of corrosion products

The acquired datasets were used in a multimodal registration [78] to fully exploit the complementary information in each dataset, allowing for segmentation of the material phases in the sample. The distribution of material phases in the sample is shown in **Paper I**, Fig. 6 for each scan. As can be seen, the proportion of corrosion products increased in scan 2, whilst the amount of free void space decreased. This observation motivated an assumption that the decrease in air void volume is due to the accumulation of uncompressed corrosion products in the air voids. Based on this assumption, an expression for the average volumetric strain in the compressed corrosion layer was derived, see Eq. (4) in **Paper I**. This average volumetric strain is calculated from the volume of compressed corrosion products, the volumetric expansion coefficient of corrosion products, the volume of steel loss, and the volume of uncompressed corrosion products. These factors can be quantified from the phase segmentation. Although the expression does not account for corrosion products leaching from cracks, it can be applied to estimate the average volumetric strain in the compressed corrosion layer in early stages of the corrosion process, when leaching of corrosion products is less pronounced [79].

3.2 Concrete cracking and kinematics

It was previously demonstrated in Sec. 3.1 how changes in material phases during the corrosion process can be linked to the average volumetric strain of corrosion products in the compressed corrosion layer. In this section, the feasibility of image-based methods to study the evolution of corrosion-induced deformations within concrete will be presented. A local Digital Volume Correlation (DVC) [80] was conducted on the neutron datasets to measure deformations induced between scans 1 and 2. In **Paper I**, Fig. 8, displacements from this local DVC were presented in a 3D vector plot together with the corrosion level along the specimen at scan 1 and 2. As observed, the damage is non-uniform and localised in regions of cracking near the end of the specimen. Interestingly, the increase in corrosion level developed between scans 1 and 2 is lower in the cracked region, suggesting that cracking was more developed in this region already after the first period of accelerated corrosion.

The first principal strain was computed from the 3D displacement field measured from the local DVC and plotted for three cross-sectional slices, see Fig. 9. in **Paper I**. In addition to these coloured cross-sectional slices of the first principal strain, the corresponding cross-section of the sample is shown. It was observed that strain localisation took place in the same regions as concrete cracking. Moreover, strain localisation took place even when the crack was not visible in the image data. Thus, this study demonstrated that the distribution of principal strains, calculated from displacements analysed from the image data using

DVC, can provide information of early stage cracking.

4 A feasibility study on X-ray Computed Tomography

The accessibility to Neutron Computed Tomography is very limited, and thus a feasibility study was conducted to investigate the applicability of local DVC measures on X-ray Computed Tomography (XCT) data. The work presented in the following was performed on XCT data from the work of Van Steen et al. [81]. The specimen analysed, B2-C1, was a cylindrical mortar specimen with a smooth steel rod subjected to accelerated corrosion. Multiple scans have been carried out at different stages during the corrosion process. In the present study, four datasets of XCT were accessed (Scan 1, Scan 2, Scan 4 and Scan 8). Scan 1 (the reference configuration) was conducted prior to the corrosion phase and the subsequent scans (deformed configurations) were executed after 166, 327 and 649 hours of exposure.

Pre-processing of the datasets was needed to ensure convergence in the subsequent DVC. First, the datasets were converted to 8 bit greyscale images and pixels were binned to reduce noise and size of the data. The image brightness was adjusted, from an upper limit of 255 to a limit of 125. A histogram equalisation was applied on the stack histogram to increase the contrast [82]. The image background and rebar was masked to exclude those from the DVC analysis. In Fig. 4.1, the adjusted dataset of the reference scan (Scan 1) is shown. The procedure applied for the local DVC was the same as in **Paper I**, using the open-source software Spam [80]. The fraction of successfully correlated subvolumes decreased slightly during the different analyses, see Tab. 4.1. During the correlation between Scans 1 and 2, the degree of successfully correlated subwindows is in close agreement with that in **Paper I** (97.5%), indicating that this type of analysis works well also on data obtained from XCT.

Table 4.1: *Number of subvolumes, window size, node spacing and fraction of converged subvolumes during the local DVC.*

	Scan 1 - Scan 2	Scan 1 - Scan 4	Scan 1 - Scan 8
Number of subvolumes	236297		
Window size (X,Y,Z) [voxels]	16, 16, 12		
Node spacing [voxels]	32, 32, 24		
Convergence [%]	97.4	96.3	92.4
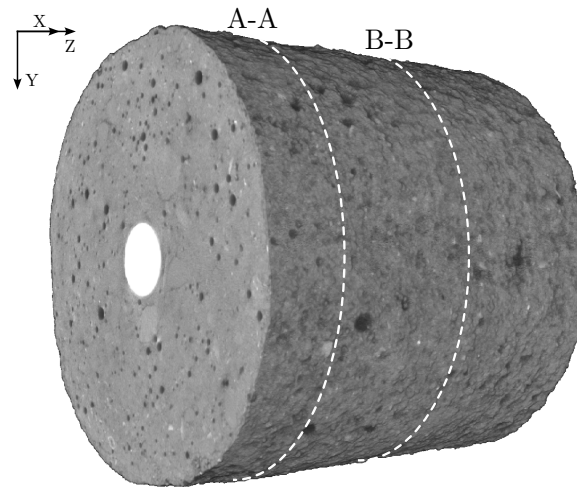
Figure 4.1: *Pre-processed XCT of B2-C1 in its uncorroded state (Scan 1).*

From the local DVC, the distribution of first principal strain was computed for each analysis. Figs. 4.2 and Figs. 4.3 show the distribution of principal strain for two different cross-sections, with locations according to Fig. 4.1. In the early stages of corrosion exposure, strain can be seen localised at the outer perimeter of the specimen, and around the steel. The reason for strain localisation at the outer perimeter of the specimen is not fully understood. However, upon examination of the images acquired at each scan, it appears that the outer surface of the specimen may have incurred damage between scans. This damage could potentially explain the observed strain localisation at the outer perimeter of the concrete. At later stages, strain localisation can be seen in correspondence with the crack pattern (Figs. 4.2d and 4.3d).
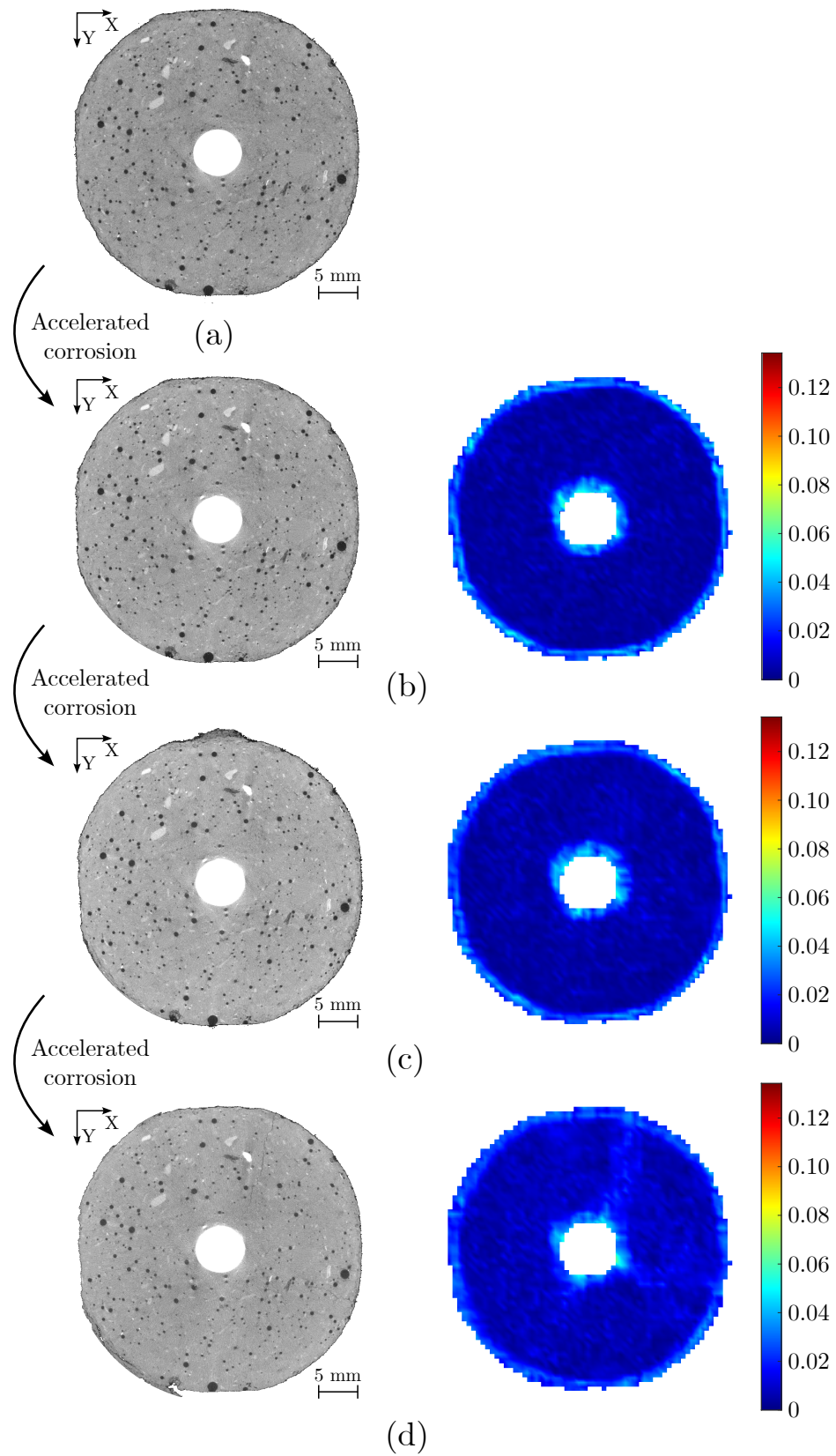
Figure 4.2: *Cross-section A-A obtained from XCT after a) Scan 1, b) Scan 2, c) Scan 4 and d) Scan 8. The corresponding distribution of first principal strain is shown to the right.*
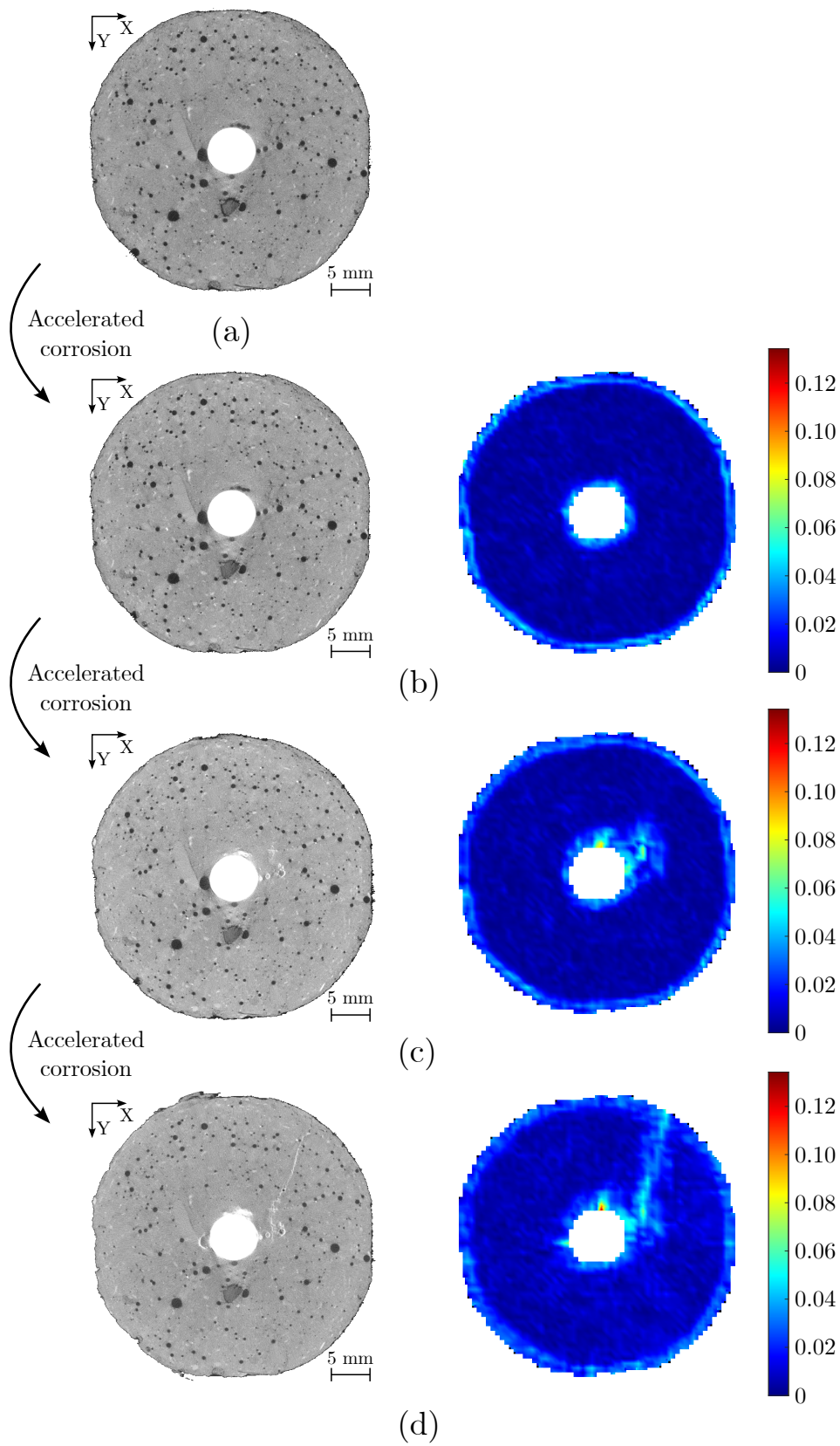
Figure 4.3: *Cross-section B-B obtained from XCT after a) Scan 1, b) Scan 2, c) Scan 4 and d) Scan 8. The corresponding distribution of first principal strain is shown to the right.*

5 A study combining strain monitoring and X-ray Computed Tomography

This Chapter refers to the work conducted in **Paper II**. In the following, the design of the experimental setup is outlined, and some key results are discussed. As elaborated in Sec. 2.4, the mechanical behaviour of corrosion products is an important part in constitutive modelling of the corrosion-induced cracking process in reinforced concrete. Hence, monitoring of the relation between stress and strain at the SCI is of major interest. In this work, an experimental setup was designed to monitor mechanical effects resulting from steel corrosion in reinforced concrete adjacent to the SCI. An experimental programme was conducted to study the relation between corrosion-induced deformations in the steel, concrete cracking and corrosion level.

Fan et al. [27] employed a distributed optical fibre sensor wound around a steel bar before casting, to monitor the time dependent expansive strains induced by corrosion. In the present work, hollow steel tubes were cast in concrete and optical fibres were utilised to monitor corrosion-induced deformations at the inner surface of the steel. This approach ensures that the corrosion process at the SCI remains unaffected by the optical fibre, thus preventing potential interference with the formation of corrosion near the fibre, possibly affecting the adhesive bond between the fibre and the steel. Additionally, the use of hollow steel bars helped mitigate beam hardening effects in the X-ray Computed Tomography (XCT) scans, performed after the corrosion period.

5.1 Design of test setup

The design of the experimental setup raised several questions that required further examination:

1. What selected geometry will enable measurable strains and sufficiently high resolution from XCT scan?

2. How can an optical fibre be mounted in a helical shape inside a steel tube?

3. How can the fibre response be validated?

4. How can corrosion be prevented from forming on the inner surface of the steel?

These questions are discussed in the following.

Choice of geometry

An important part of the experimental setup was to determine a suitable geometry of the samples (Question 1). On one hand, the smaller the sample size, the higher the resolution from XCT. On the other hand, a smaller sample size, and in particular a smaller steel tube diameter, makes the process of mounting fibres in a helical shape inside the steel tube challenging. Cylindrical samples were chosen to ease the reconstruction of the XCT data. Consequently, the geometrical parameters to be determined were the outer and inner diameter of the steel tube, the size of the concrete cover and the length of the specimen.

The outer diameter of the steel tube was chosen to 28 mm, a size that would enable removal of ribs from a 32 mm reinforcing bar and still allow for a sufficiently large inner diameter to mount the fibres. The steel wall thickness and size of concrete cover was determined based on a parameter study using finite element analysis. An axisymmetric model was created in DIANA FEA [83] with the model geometry shown in Fig. 5.1. The effect of uniform steel corrosion was considered using the corrosion model and corresponding calibration described in [58], which was assigned to the interface elements between the steel and the concrete. This corrosion model accounts for a stress dependent volume increase, due to formation of corrosion products. The effect on the reduced stiffness of the steel tube due to reduction in steel cross-sectional area is considered to be negligible. The concrete was modelled using a constitutive model based on non-linear fracture mechanics, with three radial cracks assumed. Cracking was modelled applying the smeared crack approach [84] and a total strain based crack model with rotating crack orientation. Since the crack bandwidth was dependent on the spacing between cracks, and indirectly on the radius, the concrete was divided into ten discrete elements, and each element was assigned an average value of the crack bandwidth. The material properties assigned for concrete were: Young's modulus 33 GPa, Poisson's ratio 0.2, compressive strength 38 MPa, tensile strength 2.9 MPa and the mode I fracture energy $90 \, \mathrm{N \, m^{-1}}$. The steel was modelled as an elastic ideal plastic material based on the Von Mises yield criterion, with a Young's modulus of 200 GPa, Poisson's ratio 0.3 and a yield stress 500 MPa.

The hoop strain, evaluated at the inner surface of the steel, see Fig. 5.2, was plotted as a function of the theoretical corrosion depth. Analyses were carried out for different values of the steel wall thickness (two, three and four millimetres) and concrete cover (30 mm, 40 mm and 50 mm). As can be seen, both the wall thickness of the steel tube and the concrete cover strongly affect the magnitude of the strains at the inner surface of the steel.
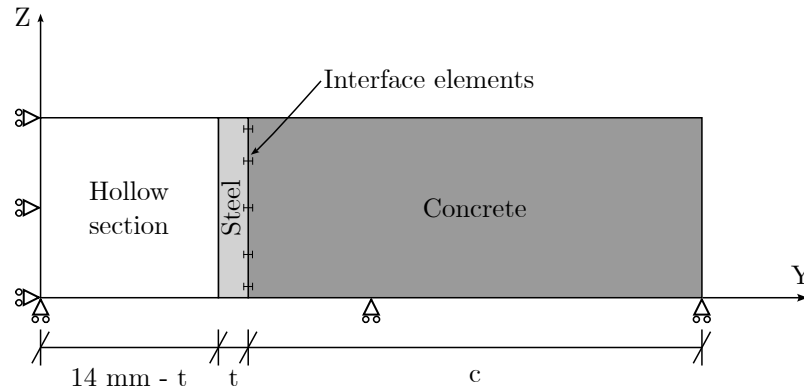
Figure 5.1: *Axisymmetric model for parameter study on steel wall thickness (t) and concrete cover (c).*
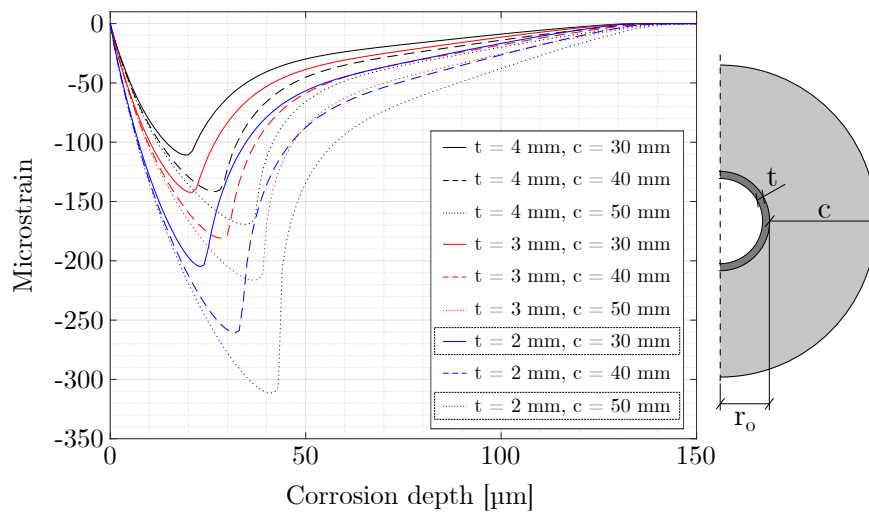

Figure 5.2: *Parameter study on the effect of different steel wall thicknesses (t) and concrete cover (c) on the corrosion-induced hoop strain at the inner surface of the steel.*

From the results in Fig. 5.2, a steel tube with a wall thickness of 2 mm resulted in high magnitudes of hoop strain and was therefore chosen. Two different concrete covers, 30 mm and 50 mm, were chosen. The length of each specimen was chosen to 100 mm, with the steel tube protruding 10 mm from the bottom surface. The geometry with the smaller concrete cover was also considered acceptable with regard to XCT.

Bonding of optical fibre in helical shape

During initial attempts to manually glue an optical fibre to the inner surface of a steel tube in a helical shape, difficulties arose, leading to the formulation of Question 2: How can an optical fibre be bonded in a helical shape inside a steel tube? Two main challenges were identified: 1) To maintain the helix of the fibre

while bonding it to the inner surface of the steel tube, and 2) to keep the distance of each turn constant. To overcome these issues, a special tool for fibre gluing was designed. The tool consisted of a steel rod with three removable plastic arms attached to it. The plastic arms were manufactured using a 3D printer. Each arm had notches spaced ten millimetres apart, where the fibre was wound, allowing for a better control of the turn height of the fibre. The fibre was thereafter secured with tape at each end of the tool. Subsequently, the tool, with the fibre attached, was placed inside the steel tube, and after that, the tape was removed. By twisting the tool, the fibre was pushed towards the inner wall of the steel tube, resulting in its helical shape, as shown in Fig. 5.3. Subsequently, the fibre was bonded to the inner steel tube by firstly gluing the parts in between each plastic arm. After curing, the tool was removed and the remaining parts of the fibre were bonded to the surface of the steel.
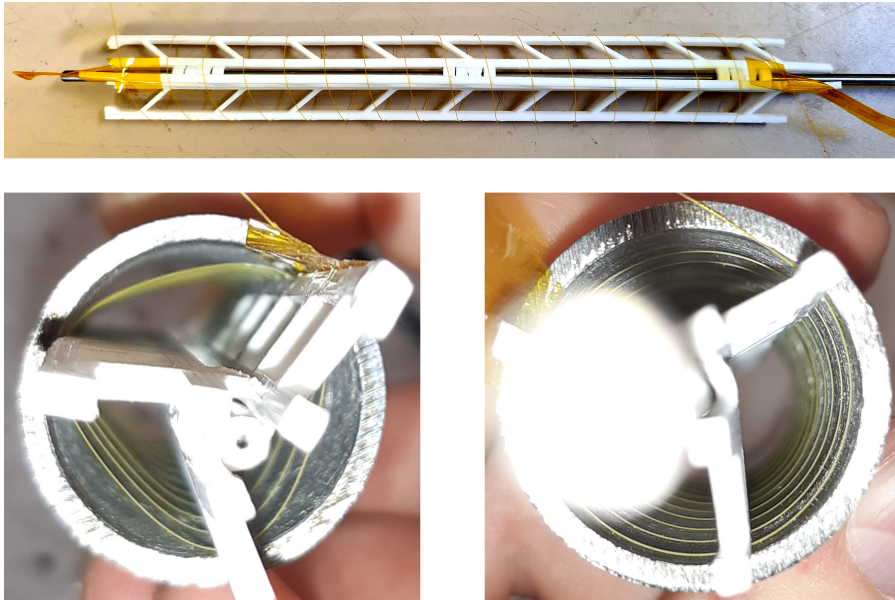
Figure 5.3: *Plastic tool for mounting of optical fibre inside a steel tube.*

Validation of strain response

To validate whether the strains measured in the distributed optical fibre were trustworthy (Question 3), a validation test was designed and conducted. In this test, a uniformly distributed pressure was applied on the outer surface of a single steel tube of the same geometry as in the corrosion experiments. To apply this uniform pressure, a pressure chamber was designed, and the steel tube was placed in it, as shown in Fig. 5.4. A hydraulic pressure was then applied whilst the distribution of strain along the fibre was measured. As can be seen in Fig. 6 in **Paper II**, the results obtained from the test showed a good agreement with numerical simulations, confirming the validity of the strain measurements.
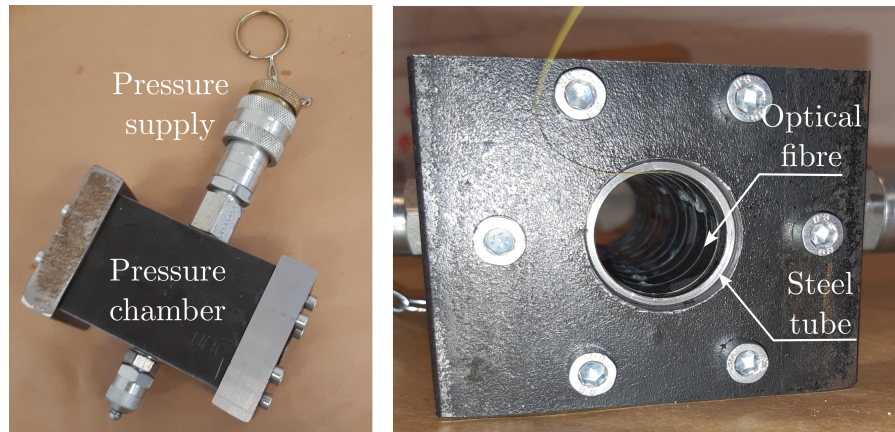
Figure 5.4: *Pressure chamber and installation of a single steel tube inside.*

Prevention of corrosion at the inner surface of the steel tubes

During the accelerated corrosion phase, the specimens were immersed in a saline solution. Corrosion was intended to take place at the interface between the steel and the concrete only. Thus, it was necessary to ensure that the inner surface of the steel tube did not corrode, as this could potentially have a detrimental effect on the fibre and affect the strain measurements. Question 4) relates with how this can be achieved; it was accomplished by preventing water from entering the inside of the steel tube. The steel tube protruded 10 mm from the bottom surface of the specimen, and passed through outlets made in the water containers to prevent water from entering the steel tube. To avoid water leakage from the container, the interface between the container and the bottom surface of the specimen was sealed with a layer of lubricant grease, as shown in Figure 5.5.

5.2 Concrete cracking, corrosion level and strain measurements

In the following, some of the key results from **Paper II** are discussed. In Fig. 7 (**Paper II**), the distribution of strain along the optical fibre after one day of impressed current is plotted for four different specimens. The strain measurements are relative to the strain at the start of the accelerated corrosion phase. As can be seen, the strains display fluctuating values, indicating non-uniform radial stress at the outer surface of the steel. XCT scans taken after the corrosion period revealed cracking in all specimens, including the reference specimens (Fig. 9 in **Paper II**) that were not subjected to accelerated corrosion. The X-ray data of the reference specimens, did not show any sign of corrosion. This was later verified through visual inspection of the sand-blasted steel in one of the reference specimens. Hence, the concrete cracking in the reference specimens was most
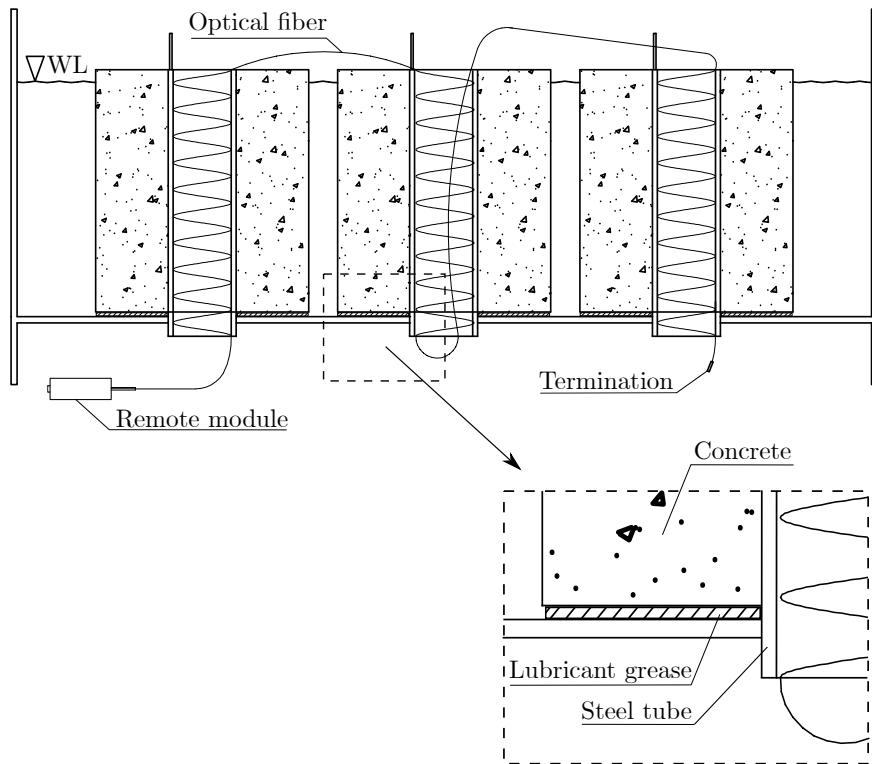
Figure 5.5: *Experimental setup for test types subjected to accelerated corrosion. The steel protruded from the bottom surface of the specimen and passed through outlets in the containers, thus preventing water entering the inside of the tubes. Water leakage was prevented by a layer of lubricant grease applied to the bottom surface of the concrete.*

likely induced by concrete shrinkage prior to the accelerated corrosion.

Corrosion was localised along the steel in correspondence with the corrosion-induced concrete cracks. In these regions, extension hoop strains were measured whilst contraction hoop strains were measured in regions of less corrosion, as seen in Fig. 12 in **Paper II**. The results are consistent with previous research that has observed a non-uniform distribution of strain around the steel [75].

6 Conclusions and outlook

6.1 Conclusions

In this work, novel approaches for monitoring effects of steel corrosion in reinforced concrete were developed and applied. One research question addressed concerned how corrosion-induced deformations within the concrete could be quantified. Time resolved multimodal Neutron and X-ray Computed Tomography (NCT and XCT) proved to be an appropriate method to study the deformations and cracking of the concrete cover in the sample. Digital Volume Correlation (DVC) of the neutron data was used to obtain quantitative measures of the corrosion-induced deformations, while combined use of NCT and XCT enabled qualitative assessment of concrete cracking. The following conclusions were drawn:

- The DVC analysis successfully quantified corrosion-induced deformations within the concrete, and the location of concrete cracking corresponded well with the observed strain localisation. Remarkably, the kinematics quantified using DVC enabled the detection of strain localisation in regions where concrete cracks were too small to be visually identified from the image data, suggesting its potential for detecting early stage concrete cracking.

- Additionally, the feasibility of using data acquired from XCT for measures on corrosion-induced deformations within concrete was investigated. It was found that DVC analysis on time-resolved XCT was capable of capturing these deformations. This finding is significant as XCT is more widely accessible compared to NCT.

A second research question addressed concerned how the evolution of material phases during corrosion can be linked to kinematics. To investigate this, time-resolved multimodal NCT and XCT techniques were combined. This allowed for segmentation of the sample into different material phases, facilitating tracking of changes in material phases between each scan. The following outcomes were reached:

- When comparing the distribution of material phases at different stages during the process, it was observed that the volume of free air voids decreased while the volume of corrosion products increased during the corrosion process.

- An expression for the average volumetric strain in the compressed corrosion layer was derived, by assuming that uncompressed corrosion products were

accommodated in air voids and that the amount of corrosion products leaching out of the specimen was negligible. This expression provides a reasonable approximation of volumetric strain at early stages of corrosion propagation.

The third research question addressed concerned how the corrosion-induced deformations in the steel can be monitored non-destructively, and in turn linked to concrete cracking and corrosion level. A novel experimental setup, that incorporated an open-ended steel tube instrumented with an optical fibre for distributed strain sensing, was designed to monitor mechanical effects resulting from steel corrosion in reinforced concrete adjacent to the steel-concrete interface. An experimental programme, in which the impact of concrete cover and prior freezing damage was varied, was conducted to study the relation between corrosion-induced deformations in the steel, concrete cracking and corrosion level. The following conclusions were drawn:

- The distribution of strain was observed to be non-uniform in all specimens included in the experimental programme, indicating a non-uniform distribution of radial stress at the steel-concrete interface. Notably, this non-uniformity correlated well with the location of the corrosion-induced cracks, with extension hoop strains observed in the steel tube at the location of these cracks, and contraction hoop strains observed in between them.

- The corrosion level exhibited variation around the perimeter of the steel, with higher values observed in vicinity of the corrosion-induced cracks.

- The thickness of the concrete cover was found to have an impact on the magnitude of strain measured in the steel, as can be expected, larger concrete cover resulted in larger strains, indicating a larger radial pressure.

- Finally, the experimental results demonstrated the potential of combining distributed optical fibres for monitoring corrosion-induced deformations in an open-ended steel tube and XCT for quantitative and qualitative measures on corrosion level and concrete cracking, respectively.

In conclusion, significant steps were taken in the development and implementation of novel approaches for non-destructive monitoring to quantify evolving physical processes involved in corrosion-induced cracking in small-scale reinforced concrete.

6.2 Future work

With the overall aim of the PhD project in mind, it would be worthwhile to continue investigating the use of time-resolved multimodal Neutron and X-ray

Computed Tomography, as these techniques have shown great potential for monitoring the effects of steel corrosion in reinforced concrete. It is recommended that multiple scans at various stages of the corrosion process are conducted, starting from the uncorroded stage. This has potential to provide valuable data on the kinematics of corrosion products. Additionally, by studying the evolution of material phases during the corrosion process, there are opportunities to investigate the influence of the corrosion accommodating region by examining the amount of uncompressed corrosion products accommodated in the air voids. This, in relation to the total volume of corrosion products, could yield valuable insights. Further, analyses aiming at tracking the mobility of corrosion products within the sample could enhance our understanding of corrosion being accommodated in air voids, as well as the impact of cracking on the transport of corrosion products.

Moreover, further analyses of data from the experimental setup proposed in this thesis (Chapter 5) could enable study of the distribution of radial stress at the steel-concrete interface. Valuable information on the mechanical properties of corrosion products formed in reinforced concrete could be gained, by combining such measure of radial stress with the volumetric strain of compressed corrosion products. However, to obtain mechanical properties of the corrosion products, strain measurements at the inside of the steel tube (to be converted to radial stress) and time-resolved combined Neutron and X-ray measurements on the same specimens are required, which will indeed include practical challenges. Regardless of the experimental strategy adopted, integration of experimental work with modelling of the corrosion-induced cracking process is vital.

References

[1] C.R. Gagg. Cement and concrete as an engineering material: An historic appraisal and case study analysis. *Engineering Failure Analysis* 40 (2014), pp. 114–140. DOI: 10.1016/j.engfailanal.2014.02.004.

[2] Z. Zhang. Research on the History and Compositions of Concrete. *Advanced Materials Research* 988 (2014), pp. 207–210. DOI: 10.4028/www.scientific.net/AMR.988.207.

[3] J.K Wight. *Reinforced concrete Mechanics and Design.* Seventh Edition. Pearson Eductional Limited, Edinburgh Gate, England, 2016.

[4] A. Poursaee and C.M. Hansson. Potential pitfalls in assessing chloride-induced corrosion of steel in concrete. *Cement and Concrete Research* 39 (2009), pp. 391–400. DOI: 10.1016/j.cemconres.2009.01.015.

[5] M. Raupach. Chloride-induced macrocell corrosion of steel in concrete - theoretical background and practical consequences. *Construction and Building Materials* 10.5 (1996), pp. 329–338.

[6] R Capozucca. Damage to reinforced concrete due to reinforcement corrosion. *Construction and Building Materials* 9 (1995).

[7] AMPP. *Highways and Bridges.* 2023. URL: https://www.ampp.org/technical-research/what-is-corrosion/corrosion-reference-library/highways-bridges (visited on 02/14/2023).

[8] B. Hou et al. The cost of corrosion in China. *npj Materials Degradation* 1.4 (2018). DOI: 10.1038/s41529-017-0005-2.

[9] I. Yoon, O. Çopuroğlu, and K. Park. Effect of global climatic change on carbonation progress in concrete. *Atmospheric Environment* 11 (2007), pp. 7274–7285. DOI: 10.1016/j.atmosenv.2007.05.028.

[10] M. Stewart, X. Wang, and M. Nguyen. Climate change impact and risks of concrete infrastructure deterioration. *Engineering Structures* 4 (2011), pp. 1326–1337. DOI: 10.1016/j.engstruct.2011.01.010.

[11] E. Bastidas-Arteaga, F. Schoefs, M. Stewart, and X. Wang. Influence of global warming on durability of corroding RC structures: A probabilistic approach. *Engineering Structures* 51 (2013), pp. 259–266. DOI: 10.1016/j.engstruct.2013.01.006.

[12] A. Nasr, D. Honfi, and O. Larsson Ivanov. Probabilistic analysis of climate change impact on chloride-induced deterioration of reinforced concrete considering Nordic climate. *Journal of Infrastructure Preservation and Resilience* 3 (2022). DOI: 10.1186/s43065-022-00053-6.

[13] B. Elsener, C. Andrade, J. Gulikers, R. Polder, and M. Raupach. Half-cell potential measurements - Potential mapping on reinforced concrete structures. *Materials and Structures* 36.261 (2003), pp. 461–471.

[14] H-W. Song and V. Saraswathy. Corrosion Monitoring of Reinforced Concrete Structures - A Review. *International Journal of Electrochemical Science* 2 (2007), pp. 1–28.

[15] C. Andrade et al. Test methods for on-site corrosion rate measurement of steel reinforcement in concrete by means of the polarization resistance method. *Materials and Structures* 37 (2004), pp. 623–643.

[16] Ueli M. Angst. Challenges and opportunities in corrosion of steel in concrete. *Materials and Structures* 51 (2018). DOI: 10.1617/s11527-017-1131-6.

[17] C. Andrade, C. Alonso, and F. J. Molina. Cover cracking as a funcion of bar corrosion: Part I - Experimental test. *Materials and Structures* 26 (1993), pp. 453–464. DOI: 10.1007/BF02472805.

[18] J. G. Cabrera. Deterioration of concrete due to reinforcement steel corrosion. *Cement and Concrete Composites* 18 (1996), pp. 47–59. DOI: 10.1016/0958-9465(95)00043-7.

[19] C. Alonso, C. Andrade, J. Rodriguez, and J. M. Diez. Factors controlling cracking of concrete affected by reinforcement corrosion. *Materials and Structures* 31 (1998), pp. 435–441. DOI: 10.1007/bf02480466.

[20] C. Andrade, A. Cesetti, G. Mancini, and F. Tondolo. Estimating corrosion attack in reinforced concrete by means of crack opening. *Structural Concrete* 17.4 (2016), pp. 533–540. DOI: 10.1002/suco.201500114.

[21] M. Tahershamsi, I. Fernandez, K. Lundgren, and K. Zandi. Investigating correlations between crack width, corrosion level and anchorage capacity. *Structure and Infrastructure Engineering* 13.10 (2017), pp. 1294–1307. DOI: 10.1080/15732479.2016.1263673.

[22] F. U. A. Shaikh. Effect of Cracking on Corrosion of Steel in Concrete. *International journal of Concrete Structures and Materials* 12 (2018). DOI: 10.1186/s40069-018-0234-y.

[23] E. Chen, C. G. Berrocal, I. Löfgren, and K. Lundgren. Correlation between concrete cracks and corrosion characteristics of steel reinforcement in pre-cracked plain and fibre-reinforced concrete beams. *Materials and Structures* 53 (2020). DOI: 10.1617/s11527-020-01466-z.

[24] C. G. Berrocal, I. Fernandez, and R. Rempling. The interplay between corrosion and cracks in reinforced concrete beams with non-uniform reinforcement corrosion. *Materials and Structures* 55 (2022). DOI: `10.1617/s11527-022-01956-2`.

[25] G. Fang, W. Ding, Y. Liu, J. Zhang, F. Xing, and B. Dong. Identification of corrosion products and 3D distribution in reinforced concrete using X-ray micro computed tomography. *Construction and Building Materials* 207 (2019), pp. 304–315. ISSN: 0950-0618. DOI: `10.1016/j.conbuildmat.2019.02.133`.

[26] S. Robuschi, A. Tengattini, J. Dijkstra, I. Fernandez, and K. Lundgren. A closer look at corrosion of steel reinforcement bars in concrete using 3D neutron and X-ray computed tomography. *Cement and Concrete Research* 144 (2021). DOI: `10.1016/j.cemconres.2021.106439`.

[27] L. Fan, X. Tan, Q. Zhang, W. Meng, G. Chen, and Y. Bao. Monitoring corrosion of steel bars in reinforced concrete based on helix strains measured from a distributed fiber optic sensors. *Engineering Structures* 204 (2020). DOI: `10.1016/j.engstruct.2019.110039`.

[28] Carolyn M. Hansson. Comments on electrochemical measurements of the rate of corrosion of steel in concrete. *Cement and Concrete Research* 14 (1984), pp. 574–584.

[29] M. Raupach. Investigations on the influence of oxygen on corrosion of steel in concrete - Part I. *Materials and Structures* 29 (1996), pp. 174–184.

[30] M. Pourbaix and R.W. Staehle. *Electrochemical Equilibria. In: Lectures on Electrochemical Corrosion.* Springer New York, NY, 1973. DOI: `10.1007/978-1-4684-1806-4_4`.

[31] Kyøsti Tuutti. *Corrosion of steel in concrete.* Stockholm: Swedish Cement and Concrete Research Institute, 1982. URL: `http://www.cbi.se/viewNavMenu.do?menuID=317&oid=857`.

[32] R. Rodrigues, S. Gaboreau, J. Gance, I. Ignatiadis, and S. Betelu. Reinforced concrete structures: A review of corrosion mechanisms and advances in electrical methods for corrosion monitoring. *Construction and Building Materials* 269 (2021). DOI: `10.1016/j.conbuildmat.2020.121240`.

[33] T. Zhang and O.E. GjØrv. Diffusion behavior of chloride ions in concrete. *Cement and Concrete Research* 26.6 (1996), pp. 907–917. DOI: `10.1016/0008-8846(96)00069-5`.

[34] U. Angst, B. Elsener, C.K. Larsen, and Ø. Vennesland. Critical chloride content in reinforced concrete - A review. *Cement and Concrete Research* 39 (2009). DOI: `10.1016/j.cemconres.2009.08.006`.

[35] M.G. Stewart and A. Al-Harthy. Pitting corrosion and structural reliability of corroding RC structures: Experimental data and probabilistic analysis. *Reliability Engineering and System Safety* 93 (2008), pp. 373–382. DOI: `10.1016/j.ress.2006.12.013`.

[36] Y. Zhou, Gencturk B., K. William, and A. Attar. Carbonation-Induced and Chloride-Induced Corrosion in Reinforced Concrete Structures. *Journal of Materials in Civil Engineering* 27.9 (2014).

[37] L.J. Parrott. Damage caused by carbonation of reinforced concrete. *Materials and Structures* 23 (1990), pp. 230–234.

[38] Y. Yuan, Y. Ji, and S.P. Shah. Comparison of Two Accelerated Corrosion Techniques for Concrete Structures. *ACI Structural Journal* 104.3 (2007).

[39] S. Ahmad. Techniques for inducing accelerated corrosion of steel in concrete. *Arabian Journal for Science and Engineering* 34.2C (2009), 95–104.

[40] W. Feng, A. Tarakbar, S.A. Memon, W. Tang, and H. Cui. Methods of accelerating chloride-induced corrosion in steel-reinforced concrete: A comparative review. *Construction and Building Materials* 289 (2021), p. 123165. DOI: `10.1016/j.conbuildmat.2021.123165`.

[41] W. Zhang, X. Song, X. Gu, and S. Li. Tensile and fatigue behavior of corroded rebars. *Construction and Building Materials* 34 (2012), pp. 409–417. DOI: `10.1016/j.conbuildmat.2012.02.071`.

[42] C. Lu, S. Yuan, P. Cheng, and R. Liu. Mechanical properties of corroded steel bars in pre-cracked concrete suffering from chloride attack. *Construction and Building Materials* 123 (2016), pp. 649–660. DOI: `10.1016/j.conbuildmat.2016.07.032`.

[43] E. Chen, C.G. Berrocal, I. Löfgren, and K. Lundgren. Corrosion Pattern and Mechanical behaviour of Corroded Rebars in Cracked Plain and Fibre Reinforced Concrete. *Fibre Reinforced Concrete: Improvements and Innovations* 30 (2021). DOI: `10.1007/978-3-030-58482-5_44`.

[44] Y.G. Du, L.A. Clark, and A.H.C. Chan. Effect of corrosion on ductility of reinforcing bars. *Magazine of Concrete Research* 57.7 (2005), pp. 407–419. DOI: `10.1680/macr.2005.57.7.407`.

[45] J. Rodriguez, L.M. Ortega, and A.M. Garcia. Assessment of Structural Elements with Corroded Rebars. *Corrosion and corrosion protection of steel in concrete* 1 (1994), pp. 171–185.

[46] K. Lundgren. Effect of corrosion on the bond between steel and concrete: an overview. *Magazine of Concrete Research* 59.6 (2007), pp. 447–461. DOI: `10.1680/macr.2007.59.6.447`.

[47] A. Poursaee and B. Ross. The Role of Cracks in Chloride-Induced Corrosion of Carbon Steel in Concrete - Review. *Corrosion and Materials Degradation* 3.2 (2022), pp. 258–269. DOI: 10.3390/cmd3020015.

[48] E. Chen, C.G. Berrocal, I. Fernandez, I Löfgren, and K. Lundgren. Assessment of the mechanical behaviour of reinforcement bars with localised pitting corrosion by Digital Image Correlation. *Engineering Structures* 219 (2020), p. 110936. DOI: 10.1016/j.engstruct.2020.110936.

[49] S. Robuschi, O. Larsson Ivanov, M. Geiker, and K. Lundgren. Impact of cracks on distribution of chloride-induced reinforcement corrosion. *Materials and Structures* 56.7 (2023). DOI: 10.1617/s11527-022-02085-6.

[50] W. Li, W. Liu, and S. Wang. The Effect of Crack Width on Chloride-Induced Corrosion of Steel in Concrete. *Advances in Material Science and Engineering* 2017.3968578 (2017). DOI: 10.1155/2017/3968578.

[51] R. François and G. Arliguie. Influence of Service Cracking on Reinforcement Steel Corrosion. *Journal of Materials in Civil Engineering* 10.1 (1998), pp. 14–20. DOI: 10.1061/(ASCE)0899-1561(1998)10:1(14).

[52] R. François and G. Arliguie. Effect of microcracking and cracking on the development of corrosion in reinforced concrete members. *Magazine of Concrete Research* 51.2 (1999), pp. 143–150. DOI: 10.1680/macr.1999.51.2.143.

[53] R.J. Zhang, A. Castel, and R. François. Effect of corrosion pattern on RC beam performance. *Proceedings of the Institution of Civil Engineers - Construction Materials* 163.2 (2010), pp. 97–108. DOI: 10.1680/coma.2010.163.2.97.

[54] A. Poursaee and C.M. Hansson. The influence of longitudinal cracks on the corrosion protection afforded reinforcing steel in high performance concrete. *Cement and Concrete Research* 38 (2008), pp. 1098–1105. DOI: 10.1016/j.cemconres.2008.03.018.

[55] C. Cao, M.M.S. Cheung, and B.Y.B Chan. Modelling of interaction between corrosion-induced concrete cover crack and steel corrosion rate. *Corrosion Science* 69 (2013), pp. 97–109. DOI: 10.1016/j.corsci.2012.11.028.

[56] Zdenžk P. Bažant. Physical Model for Steel Corrosion in Concrete Sea Structures - Application. *Journal of Structural Division* 105 (6 1979), pp. 1155–1166. DOI: 10.1061/JSDEAG.0005169.

[57] Y. Liu and R.E. Weyers. Modeling the Time-to-Corrosion Cracking in Chloride Contaminated Reinforced Concrete Structures. *ACI Materials Journal* 95.6 (1998), pp. 675–681. DOI: 10.14359/410.

[58] K. Lundgren. Bond between ribbed bars and concrete. Part 2: The effect of corrosion. *Magazine of Concrete Research* 57.7 (2005), pp. 383–395.

[59]   J. Ožbolt, F. Oršanic, and G. Balabanić. Modeling damage in concrete caused by corrosion of reinforcement: coupled 3D FE model. *International Journal of Fracture* 178 (2012), pp. 233–244. DOI: 10.1007/s10704-012-9774-3.

[60]   C. Andrade, F. Tavares, L. Toro, and J. Fullea. "Observations on the Morphology of Oxide Formation due to Reinforcement Corrosion". *Modelling of Corroding Concrete Structures*. Springer, Netherlands, 2011, pp. 179–193. DOI: 10.1007/978-94-007-0677-4_12.

[61]   C. Cao. 3D simulation of localized steel corrosion in chloride contaminated reinforced concrete. *Construction and Building Materials* 72 (2014), pp. 434–443. DOI: 10.1016/j.conbuildmat.2014.09.030.

[62]   B. Šavija, M. Luković, J. Pacheco, and E. Schlangen. Cracking of the concrete cover due to reinforcement corrosion: A two-dimensional lattice model study. *Construction and Building Materials* 44 (2013), pp. 626–638. ISSN: 0950-0618. DOI: 10.1016/j.conbuildmat.2013.03.063.

[63]   E. Chen and C. K.Y Leung. Finite element modeling of concrete cover cracking due to non-uniform steel corrosion. *Engineering Fracture Mechanics* 134 (2015), pp. 61–78. ISSN: 0013-7944. DOI: 10.1016/j.engfracmech.2014.12.011.

[64]   A. Ouglova, Y. Berthaud, M. François, and F. Foct. Mechanical properties of an iron oxide formed by corrosion in reinforced concrete structures. *Corrosion Science* 48.12 (2006), pp. 3988–4000. ISSN: 0010-938X. DOI: 10.1016/j.corsci.2006.03.007.

[65]   Y. Zhao, H. Dai, H. Ren, and W. Jin. Experimental study of the modulus of steel corrosion in a concrete port. *Corrosion Science* 56 (2012), pp. 17–25. ISSN: 0010-938X. DOI: 10.1016/j.corsci.2011.11.004.

[66]   F.J. Molina, C. Alonso, and C. Andrade. Cover cracking as a function of rebar corrosion: Part 2 - Numerical model. *Materials and Structures* 26 (1993), pp. 532–548. DOI: 10.1007/BF02472864.

[67]   A. Michel, B.J. Pease, M.R. Geiker, H. Stang, and J.F. Olesen. Monitoring reinforcement corrosion and corrosion-induced cracking using non-destructive x-ray attenuation measurements. *Cement and Concrete Research* 41.11 (2011), pp. 1085–1094. ISSN: 0008-8846. DOI: 10.1016/j.cemconres.2011.06.006.

[68]   A. Jamali, U. Angst, B. Adey, and B. Elsener. Modeling of corrosion-induced concrete cover cracking: A critical analysis. *Construction and Building Materials* 42 (2013), pp. 225–237. ISSN: 0950-0618. DOI: 10.1016/j.conbuildmat.2013.01.019.

[69] S. Rasheeduzzafar, S. Al-Saadoun, and S. Al-Gahtani. Corrosion Cracking in Relation to Bar Diameter, Cover and Concrete Quality. *Journal of Materials in Civil Engineering* 4.4 (1992), pp. 327–342. DOI: 10.1061/(ASCE)0899-1561(1992)4:4(327).

[70] U.M. Angst and B. Elsener. The size effect in corrosion greatly influences the predicted life span of concrete infrastructures. *Science Advances* 3.8 (2017). DOI: 10.1126/sciadv.1700751.

[71] U.E. Angst et al. The steel-concrete interface. *Materials and Structures* 50.143 (2017). DOI: 10.1617/s11527-017-1010-1.

[72] S. Brisard, M. Serdar, and P.J.M. Monteiro. Multiscale X-ray tomography of cementitious materials: A review. *Cement and Concrete Research* 128 (2020), p. 105824. ISSN: 0008-8846. DOI: 10.1016/j.cemconres.2019.105824.

[73] A. Tengattini, N. Lenoir, E. Andò, and G. Viggiani. Neutron imaging for geomechanics: A review. *Geomechanics for Energy and the Environment* 27 (2021), p. 100206. ISSN: 2352-3808. DOI: 10.1016/j.gete.2020.100206.

[74] M. Beck, J. Goebbels, and A. Burkert. Application of X-ray tomography for the verification of corrosion processes in chloride contaminated mortar. *Materials and Corrosion* 58.3 (2007), pp. 207–210. DOI: 10.1002/maco.200604049.

[75] A. Michel, B.J. Pease, A. Peterová, M.R. Geiker, H. Stang, and A.E.A. Thybo. Penetration of corrosion products and corrosion-induced cracking in reinforced cementitious materials: Experimental investigations and numerical simulations. *Cement and Concrete Composites* 47 (2014), pp. 75–86. ISSN: 0958-9465. DOI: 10.1016/j.cemconcomp.2013.04.011.

[76] B. Šavija, M. Luković, S.A.S. Hosseini, J. Pacheco, and E. Schlangen. Corrosion induced cover cracking studied by X-ray computed tomography, nanoindentation, and energy dispersive X-ray spectrometry (EDS). *Materials and Structures* 48 (2015), pp. 2043–2062. DOI: 10.1617/s11527-014-0292-9.

[77] H. Sun et al. Monitoring of steel corrosion and cracking in cement paste exposed to combined sulfate-chloride attack with X-ray microtomography. *Construction and Building Materials* 302 (2021), p. 124345. ISSN: 0950-0618. DOI: 10.1016/j.conbuildmat.2021.124345. URL: https://www.sciencedirect.com/science/article/pii/S0950061821021048.

[78] F. Maes, A. Collignon, D. Vandermeulen, G. Marchal, and P. Suetens. Multimodality Image Registration by Maximization of Mutual Information. *IEEE Transactions on Medical Imaging* 16 (1997), pp. 187–198. DOI: 10.1109/42.563664.

[79] C. Fahy, S.J. Wheeler, D. Gallipoli, and P. Grassl. Corrosion induced crack-
      ing modelled by a coupled transport-structural approach. *Cement and Con-
      crete Research* 94 (2017), pp. 24–35. ISSN: 0008-8846. DOI: 10.1016/j.
      cemconres.2017.01.007.

[80] O. Stamati et al. spam: Software for Practical Analysis of Materials. *Journal
      of Open Source Software* 5.51 (2020), p. 2286. DOI: 10.21105/joss.02286.

[81] C. Van Steen, L. Pahlavan, M. Wevers, and E. Verstrynge. Localisation
      and characterisation of corrosion damage in reinforced concrete by means
      of acoustic emission and X-ray computed tomography. *Construction and
      Building Materials* 197 (2019), pp. 21–29. DOI: 10.1016/j.conbuildmat.
      2018.11.159.

[82] C. Schneider, W. Rasband, and K Eliceiri. NIH Image to ImageJ: 25 years
      of image analysis. *Nature Methods* 9 (2012), pp. 671–675. DOI: 10.1038/
      nmeth.2089.

[83] D. Ferreira. *Diana User's Manual: Release 10.5.* 2023. URL: https://
      manuals.dianafea.com/d105/Diana.html.

[84] J.G. Rots, P. Nauta, G.M.A. Kusters, and J. Blaauwendraad. Smeared Crack
      Approach and Fracture Localization in Concrete. *HERON* 30.1 (1985). ISSN:
      0046-7316.